Biophysical Journal Volume 102 March 2012 1204–1214

In Vivo Imaging of the Actin Polymerization State with Two-Photon Fluorescence Anisotropy

Harshad D. Vishwasrao,[†‡] Pierre Trifilieff,[†§¶] and Eric R. Kandel[†‡‖*]

[†]Department of Neuroscience, Columbia University, New York, New York; [‡]Howard Hughes Medical Institute, New York, New York; [§]New York State Psychiatric Institute, New York, New York; [¶]Research Foundation for Mental Hygiene, New York, New York; and [‖]Kavli Institute for Brain Science, New York, New York

ABSTRACT Using two-photon fluorescence anisotropy imaging of actin-GFP, we have developed a method for imaging the actin polymerization state that is applicable to a broad range of experimental systems extending from fixed cells to live animals. The incorporation of expressed actin-GFP monomers into endogenous actin polymers enables energy migration FRET (emFRET, or homoFRET) between neighboring actin-GFPs. This energy migration reduces the normally high polarization of the GFP fluorescence. We derive a simple relationship between the actin-GFP fluorescence polarization anisotropy and the actin polymer fraction, thereby enabling a robust means of imaging the actin polymerization state with high spatiotemporal resolution and providing what to the best of our knowledge are the first direct images of the actin polymerization state in live, adult brain tissue and live, intact *Drosophila* larvae.

INTRODUCTION

Actin exists in cells in a dynamic equilibrium between monomeric and polymeric forms: g-actin and f-actin, respectively. Polymeric f-actin constitutes one of the principle components of the cytoskeleton and is involved in molecular scaffolding, cell motility, and myosin-based trafficking. Monomeric g-actin, on the other hand, exists as a cell-wide pool that serves as a ready source or sink of monomeric subunits to and from f-actin. The dynamic equilibrium between the two forms of actin is regulated by the cell locally, rapidly, and bidirectionally.

Given the central role for actin dynamics in a broad spectrum of cell function, it is of considerable interest to be able to image the polymerization state in live cells and tissues with high spatial and temporal resolution. Despite this need, there are few robust methods for directly imaging the actin polymerization state.

Methods for probing the actin polymerization state can be categorized either as indirect (utilizing a nonactin fluorescent probe that binds polymeric f-actin), or direct (utilizing fluorescently labeled actin). Phalloidin staining, an indirect probe, represents the gold-standard for labeling f-actin; however, it can only be applied to fixed cells and tissue, and therefore provides limited information about dynamics. A number of live cell indirect probes have been developed that we will return to in the Discussion.

Among the direct probes of actin polymerization, single-molecule-based techniques such as fluorescence speckle microscopy (1) and photoactivation localization microscopy (2) are most informative in cultured cells, but are computationally intensive and difficult to extend to live tissue.

The most broadly applicable approach to directly probe the actin polymerization state utilizes Förster resonance energy transfer (FRET) between coexpressed actin-CFP and actin-YFP. Incorporation of actin-CFP and actin-YFP into endogenous f-actin occasionally brings CFP and YFP into close proximity (<100 Å), resulting in FRET and an enhancement in the YFP/CFP fluorescence ratio. This approach has been applied in solutions of purified protein (3,4) as well as in tissue culture (5). For clarity, we will refer to the physical process of excitation energy transfer between any two molecules as "FRET" and the technique that utilizes energy transfer specifically between different fluorophores as "heteroFRET".

We present here an imaging method and analytical framework that utilizes energy migration FRET (6,7) (emFRET; also called homoFRET, homotransfer, energy migration) to directly probe the actin polymerization state quantitatively. EmFRET, like heteroFRET, is based on a resonant transfer of electronic excitation energy between two or more fluorophores. Unlike heteroFRET, emFRET occurs between fluorophores of the same type if the absorption and emission spectra overlap. Because the interacting fluorophores are identical, emFRET does not change the fluorescence color or lifetime ((7–10), and see Section S1 in the Supporting Material). However, because the emission dipoles of interacting fluorophores are seldom exactly parallel, emFRET does change the fluorescence polarization and can therefore be detected by polarization-sensitive modalities. The advantages of a single fluorophore technique such as emFRET over a dual fluorophore technique such as heteroFRET are numerous, including simplicity of experimental design, efficiency of FRET pair formation, and the potential for using already existing transgenic animals expressing actin-GFP. We will expand upon this comparison in the Discussion.

EmFRET has been used extensively to study the aggregation and structure of purified, labeled proteins. Its use in cells, although less common (for review, see Chan et al. (11)), has seen a number of promising applications and

Submitted October 5, 2011, and accepted for publication January 17, 2012.

*Correspondence: erk5@columbia.edu

Editor: Elizabeth Rhoades.

0006-3495/12/03/1204/11 $2.00

doi: 10.1016/j.bpj.2012.01.031

seminal developments of the experimental and theoretical tools necessary to derive information about intracellular molecular structure from images of emFRET-induced fluorescence depolarization (7,9–13). Much of the interest in these studies has been to extract oligomer structural parameters, for which time-resolved anisotropy measurements provide the most detailed information. Because a lifetime image typically requires minutes to acquire, this approach is of limited utility in imaging fast cellular dynamics (<10 s).

Our purpose is not to obtain structural details of f-actin, but rather to image the actin polymer fraction with a resolution sufficient to observe its characteristic rapid and highly localized dynamics in live cells, including neurons and their synapses. To this end, we employ steady-state two-photon anisotropy imaging to provide the requisite high spatiotemporal resolution. We also derive a relationship between anisotropy and the actin polymer fraction with which we can calculate images that are proportional to the actin polymer concentration. This relationship can be validated using f-actin specific stains. Although two-photon excitation is not necessary for anisotropy imaging, it provides a greater dynamic range for anisotropy due to enhanced excitation photoselection and it enables the technique to be easily extended from fixed cells to living tissue.

METHODS

See Sections S7–S12 in the Supporting Material.

RESULTS

Theoretical relationship between fluorescence anisotropy and the actin polymerization state

Actin-GFP fluorescence is highly polarized. This polarization is altered when actin-GFP incorporates into an endogenous actin polymer and undergoes FRET with other nearby incorporated molecules of actin-GFP. Although we empirically measure the fluorescence polarization anisotropy of actin-GFP, we are ultimately interested in its polymerization state. We must therefore derive the relationship between anisotropy and polymerization state.

Energy transfer between polymer-incorporated actin-GFP

Consider an actin polymer of sites *-M* to *N* with actin-GFP randomly incorporated into it (Fig. 1 *A*). Any two actin-GFP occupied sites *j*,*k* are capable of FRET with a rate F_{jk},

$$F_{jk} = \frac{3R_0^6}{2\tau}\frac{\kappa_{jk}^2}{\left|\vec{R}_{jk}\right|^6}, \qquad (1)$$

where $\vec{R}_{jk} = \vec{R}_k - \vec{R}_j$ is the vector between the two chromophores and the orientation factor,

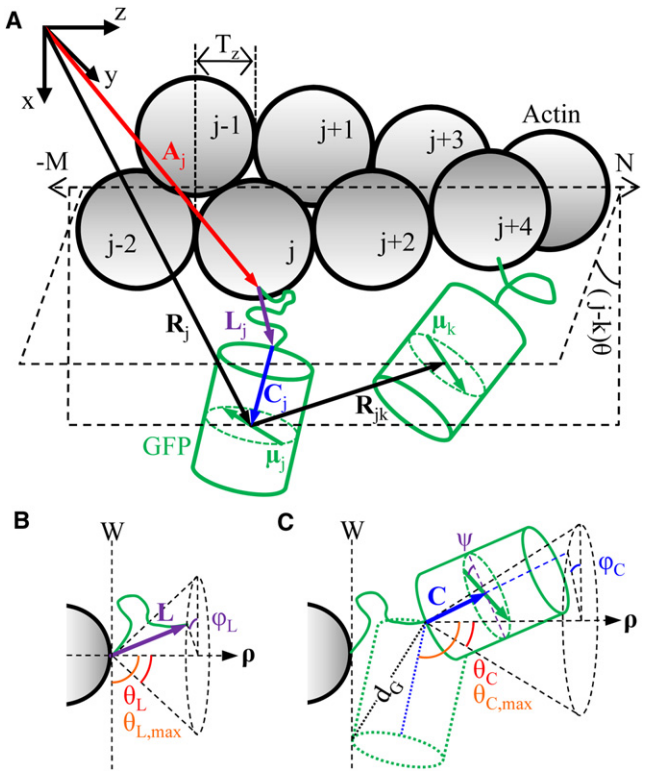

FIGURE 1 (*A*) Model of actin-GFP molecules randomly incorporated into an actin filament. (*B*) The long flexible linker (*green line*) connecting actin to GFP has an en-to-end vector **L** (*purple arrow*) with orientation angles θ_L and φ_L. (*C*) The GFP chromophore vector **C** (*blue arrow*) rotates freely at the end of the linker with orientation angles θ_C and φ_C. The orientation angles are with respect to the local helix radius vector at the actin N-terminus, **ρ**. The tangent plane *W* is a noninteracting wall; both the linker and chromophore vectors are allowed to move outside (to the right of) this wall. The GFP barrel drawn with the green dotted line in panel *C* represents the limit of motion for the GFP tag—the GFP semidiagonal d_G cannot cross *W*.

$$\kappa_{jk}^2 = \left(\left(\hat{\mu}_j \cdot \hat{\mu}_k\right) - 3\left(\hat{\mu}_j \cdot \hat{R}_{jk}\right)\left(\hat{\mu}_k \cdot \hat{R}_{jk}\right)\right)^2,$$

accounts for the relative orientation of the unit transition dipoles $\hat{\mu}_j$ and $\hat{\mu}_k$. For the GFP mutant used in most of the experiments presented here (Emerald-GFP), the fluorescence lifetime (τ) was found to be 2.49 ± 0.05 ns (see Section S1 in the Supporting Material) and the GFP-GFP Förster radius (R_0) was calculated to be 45.8 Å in tissue (refractive index 1.4), comparable to that for GFP-GFP (46.5 Å) and CFP-YFP (49.2 Å) in solution (14).

F-actin is a helix in which adjacent monomers are rotated by an angle $\theta = 166^\circ$ with respect to one another and axially offset by $A_z = 27.5$ Å. This well-defined structure relates the position of an actin N-terminus (where GFP is attached), $\vec{A}_j$, to its site index number *j* (3,15),

$$\vec{A}_j = A_{xy}\, cos(j\theta)\hat{x} + A_{xy}\, sin(j\theta)\hat{y} + A_z j\hat{z}, \qquad (2)$$

where $A_{xy} = 35$ Å is the radial distance of the N-terminus from the helix axis.

The actin N-terminus is attached to GFP by an 8 aa flexible linker. Moreover, the C-terminal 10 residues of Emerald-GFP have no secondary structure and are linked to the GFP β-barrel at a glycine residue (Gly^{229}). We therefore model actin-GFP as two rigid structures (actin and GFP(1–229)) linked by an 18-amino-acid, unstructured polypeptide chain (see Section S2 in the Supporting Material). An unstructured polypeptide chain whose contour length ($l_c = 68.4$ Å for 18 aa) greatly exceeds its persistence length ($l_p = 3.04$ Å (16)) can be modeled as a Gaussian chain with an end-to-end vector $\vec{L}_j$ whose magnitude follows the probability distribution

$$P(L_j) = P_{L0} L_j^2 \, exp\left(\frac{-3L_j^2}{4 l_p l_c}\right), \quad (3)$$

where P_{L0} is a normalization constant. Although the contour length of the linker is long, its high flexibility makes its trajectory in space a random walk, resulting in a relatively short mean end-to-end distance ($\langle L_j \rangle = 19$ Å). Finally, if $\vec{C}_j$ is the vector from the linker attachment point at Gly^{229} to the GFP chromophore ($|\vec{C}_j| = 24$ Å, Protein DataBank entry 1GFL), then the chromophore position vectors are $\vec{R}_{j,k} = \vec{A}_{j,k} + \vec{L}_{j,k} + \vec{C}_{j,k}$ and the vector between the chromophores is

$$\vec{R}_{jk} = \vec{R}_k - \vec{R}_j = \left(\vec{A}_k + \vec{L}_k + \vec{C}_k\right) - \left(\vec{A}_j + \vec{L}_j + \vec{C}_j\right). \quad (4)$$

We treat the tangent plane at the actin N-terminus as a noninteracting wall (*dashed line W*, Fig. 1, *B* and *C*) to simulate steric hindrance from the actin filament. The linker ($\vec{L}$) and chromophore ($\vec{C}$) vectors are permitted to move freely only in the half-space outside this wall (see Section S3 in the Supporting Material).

Fluorescence and FRET occur during the lifetime of the excited state (2.5 ns for Emerald GFP), substantially faster than the rotation time of GFP (15–20 ns). Hence, any single GFP has a nearly fixed position/orientation during the evolution of a single excitation. In a typical imaging experiment, however, the pixel dwell time (1–10 μs) is long in comparison to the timescale of molecular motion and involves many excitations, while the focal volume contains many GFPs (~10^2–10^3 at 1 μM GFP concentration). Therefore, the population of excited GFPs in a focal volume, over a pixel dwell time, can be considered to sample all possible positions/orientations with respect to their parent actin filaments. To account for this in the theory below, we perform an ensemble average ($\langle x \rangle$) of fluorescence-based quantities, defined as an average over all possible positions and orientations of the interacting GFP transition dipoles (that is, over all possible lengths and orientation angles of $\vec{L}_j$, $\vec{C}_j$, and $\hat{\mu}_j$), weighted by their respective probabilities of occurrence. The ensemble average is calculated using a Monte Carlo approach (see Section S4 in the Supporting Material) similar to that used by Blackman et al. (10) in modeling concentration dependent fluorescence depolarization.

For a lone pair of interacting GFPs on an actin filament, we suppose a single excitation begins on the donor at site 0. Then the probability that the emission occurs from the acceptor at site k is known as the fractional quantum yield of site k and is simply related to the FRET rate, $\Phi_k/\Phi_{total} = F_{0k}\tau/(1 + 2F_{0k}\tau)$ (17), where Φ_{total} is the fluorescence quantum yield (0.68 for Emerald-GFP). The ensemble average fractional quantum yield, as a function of the acceptor site index $|k|$, gives us a picture of how well a pairwise FRET interaction transfers energy directly between sites on an actin filament (Fig. 2 *A*, *red diamonds*). We use the absolute value of the site index here as the actin filament is symmetric about site 0. Energy transfer from the donor at site 0 is overwhelmingly to its next-to-nearest neighbors at $|k| = 2$ and becomes negligible beyond $|k| = 4$, a conclusion that we will utilize shortly.

Energy migration in an incompletely labeled polymer

Actin-GFP competes with endogenous g-actin to incorporate into f-actin, resulting in an actin filament sporadically labeled with GFP. To account for this incomplete labeling, we modify the theory of fluorescence depolarization due to energy migration between aggregated fluorophores as originally developed by Craver and Knox (17). We define the labeling (ℓ_j) of each site j as $\ell_j = 1$ if it is occupied by actin-GFP and $\ell_j = 0$ if it is occupied by endogenous actin.

Suppose a single excitation begins on an actin-GFP at an arbitrary site that we label "0". Then the probability of

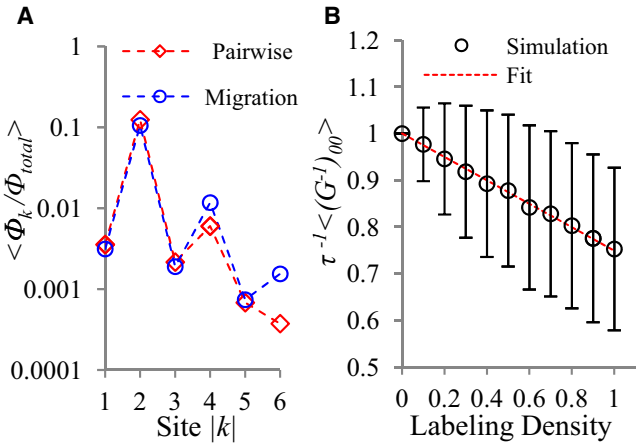

FIGURE 2 (*A*) Ensemble average fractional quantum yield as a function of site number $|k|$. Energy transfer from the initially excited site 0 directly (*Pairwise*, *red diamonds*) to another site is overwhelmingly to the $|k| = 2$ sites. On a fully labeled polymer (*Migration*, *blue circles*), the spread of excitation energy to even sites is facilitated by migration but is nonetheless restricted largely to $|k| = 2$ and 4 sites. (*B*) Simulation of a probabilistically labeled filament shows that $\tau^{-1}\langle (G^{-1})_{00} \rangle$ is linearly dependent on the labeling density ($\bar{\ell}$) of f-actin (each point is mean ± SD, 10^5 iterations).

finding an excited state at site j ($\rho_j(t)$) is governed by the master equation,

$$\frac{d\rho_j(t)}{dt} = \frac{-\rho_j(t)}{\tau} - \sum_{\substack{k=-M \\ k\neq j}}^{N} \ell_j \ell_k F_{jk} \rho_j(t) + \sum_{\substack{m=-M \\ m\neq j}}^{N} \ell_j \ell_m F_{mj} \rho_m(t), \quad (5)$$

with the temporal boundary conditions $\rho_0(t = 0) = 1$, $\rho_0(t = \infty) = 0$, and $\rho_{j\neq 0}(t = 0) = \rho_{j\neq 0}(t = \infty) = 0$. This is essentially the master equation of Craver and Knox (17) with additional $\ell_{j,k,m}$ terms to account for the incorporation of actin-GFP. The first term on the right side of the equation represents the rate of spontaneous decay, and the second and third terms, respectively, represent the FRET rate from and to site j. The summations are over all polymer sites; however, because FRET becomes negligible beyond a separation of four sites, the full summation can be approximated by a sum over k (and m) $= j-4$ to $j+4$, $\neq j$.

This system of linear differential equations can be rewritten as

$$\frac{d\rho_j(t)}{dt} = -\sum_{k=j-4}^{j+4} G_{jk} \rho_k(t), \quad (6)$$

where G_{jk} is the Craver-Knox matrix of coefficients, whose index j runs from -M to N to preserve the polymer site index notation,

$$G_{jk} = -\ell_j \ell_k F_{kj}\left(1 - \delta_{jk}\right) + \left(\frac{1}{\tau} + \sum_{\substack{m=j-4 \\ m\neq j}}^{j+4} \ell_j \ell_m F_{jm}\right)\delta_{jk}. \quad (7)$$

Once the G matrix is defined, the fractional quantum yield of site n is (8,17)

$$\frac{\Phi_n}{\Phi_{total}} = \frac{(G^{-1})_{0n}}{\tau}, \quad (8)$$

and the fluorescence anisotropy of the polymer is given by

$$\begin{aligned} r_p &= r_0 \frac{\Phi_0}{\Phi_{total}} + r_{et}\left(1 - \frac{\Phi_0}{\Phi_{total}}\right) \\ &= r_0 \frac{(G^{-1})_{00}}{\tau} + r_{et}\left(1 - \frac{(G^{-1})_{00}}{\tau}\right). \end{aligned} \quad (9)$$

Here r_0 is the anisotropy of the fluorescence arising from the initial directly excited site. Fluorescence from the initially excited site may directly follow excitation, or it may follow excitation and energy migration away from, and back to, that site. Because GFP is essentially motionless on the timescale of energy transfer, fluorescence following energy migration away from, and back to, the initially excited site will have the same polarization as if the energy had never left. Hence, the anisotropy of fluorescence from directly excited sites will be equal to that of a monomer ($r_0 \rightarrow r_m$). The value r_{et} is the anisotropy of the fluorescence from sites excited via FRET. It is generally held, and we confirm for polymer incorporated actin-GFP (see Section S5 in the Supporting Material), that even a single energy transfer is adequate to largely depolarize fluorescence, i.e., $r_{et} \rightarrow 0$ (8). Finally, because $(G^{-1})_{00}$ is defined for a specific configuration of fluorophores, the measured anisotropy from a real sample is related to the ensemble average $\langle (G^{-1})_{00} \rangle$. Equation 9 then simplifies to

$$r_p = r_m \tau^{-1} \left\langle \left(G^{-1}\right)_{00} \right\rangle. \quad (10)$$

To calculate the limits of energy migration from the initial site 0 of excitation, we simulated a seven-subunit-long polymer fully labeled on its positive sites ($\ell_j = 1$ for $0 \leq j \leq 6$) (Fig. 2 *A*, *blue circles*). By symmetry, these results apply to negative sites as well. The ensemble average fractional quantum yields for sites $|k| = 4$ and 6 on a fully labeled polymer are substantially higher than their corresponding values for direct (pairwise) FRET from the donor (Fig. 2 *A*, *red diamonds*). This indicates that energy migration (transfer via intermediary sites) to these sites can be a more efficient means of energy transfer than direct transfer. Nonetheless, energy migration was found to be highly local, with the ensemble average fractional quantum yield exceeding 1% only for sites $|k| = 2$ and 4. This acute localization of energy migration implies the anisotropy will be insensitive to the total length of the actin filament—typically hundreds of subunits or more (18,19).

Actin-GFP competes with endogenous g-actin to incorporate into actin filaments and so its incorporation probability will depend on its expression level. The probability that an actin-GFP is found at a filament site j (or the labeling density, $\overline{\ell}$) is

$$\begin{aligned} P\left(\ell_j = 1\right) &= \overline{\ell} \\ &= \frac{\mathrm{K}_{\mathrm{acGFP}}[actin - GFP]}{\mathrm{K}_{\mathrm{acGFP}}[actin - GFP] + [endogenous\ g\text{-}actin]}, \end{aligned} \quad (11)$$

where K_{acGFP} is the relative rate of incorporation of actin-GFP versus endogenous g-actin. We used a Monte Carlo simulation to average over all labeling configurations for a given labeling density (see Section S4 in the Supporting Material) to find the dependence of $\tau^{-1}\langle (G^{-1})_{00} \rangle$ and thereby the polymer anisotropy (Eq. 10), on the labeling density. Because energy transfer from the initially excited site 0 is largely restricted to the $|k| = 2$ and 4 sites even for a fully labeled polymer, we included only sites 0, ± 2, and ± 4 in the simulation. We find that the dependence of $\tau^{-1}\langle (G^{-1})_{00} \rangle$ on the labeling density (Fig. 2 *B*)

can be well fit by a straight line with a slope $m_\ell = 0.251 \pm 0.003$:

$$\tau^{-1}\left\langle \left(G^{-1}\right)_{00}\right\rangle = 1 - m_\ell \bar{\ell}. \tag{12}$$

We have fixed the intercept in the fit to be 1 because, for a negligible labeling density ($\bar{\ell} \to 0$), energy cannot transfer off site 0 and hence the fractional quantum yield of site 0 approaches the total quantum yield ($\Phi_0 \to \Phi_{total}$) and, therefore, by Eq. 8: $\tau^{-1}\langle (G^{-1})_{00}\rangle \to 1$.

Anisotropy of a mixture of monomer and polymer

For a fluorophore that exists as a mixture of monomeric and polymeric populations, the average anisotropy is simply the sum of the anisotropies of the monomer and the polymer weighted by their fractional concentrations:

$$r = \frac{C_m}{C_m + C_p} r_m + \frac{C_p}{C_m + C_p} r_p. \tag{13}$$

Here $C_{m,p}$ and $r_{m,p}$ are the concentrations and anisotropies of the monomer and polymer, respectively. Substituting the expressions for polymer anisotropy (Eq. 10) and $\tau^{-1}\langle (G^{-1})_{00}\rangle$ (Eq. 12) into Eq. 13 and solving for the polymer concentration, C_p, gives the final expression for the anisotropy of a monomer/polymer mixture,

$$\begin{aligned} C_p &= \left(\frac{1}{1 - \tau^{-1}\left\langle \left(G^{-1}\right)_{00}\right\rangle}\right)\left(1 - \frac{r}{r_m}\right) C_T \\ &= \frac{1}{m_\ell \bar{\ell}}\left(1 - \frac{r}{r_m}\right) C_T, \end{aligned} \tag{14}$$

where $C_T = C_m + C_p$ is the total actin-GFP concentration. Although $\tau^{-1}\langle (G^{-1})_{00}\rangle$ or m_ℓ can be explicitly calculated as we have shown above, for most experimental purposes it is enough to note from Eqs. 1–4, 7, and 11 that $\tau^{-1}\langle (G^{-1})_{00}\rangle$ is solely determined by three sets of parameters:

1. Fluorophore parameters: R_0, r_m, $|\vec{C}|$, and $|\vec{L}|$.
2. F-actin structure parameters: A_{xy}, A_z, θ, and filament length ($M + N + 1$).
3. Expression level: $\bar{\ell}$.

Because every term of G contains τ^{-1}, the explicit dependence of $\tau^{-1}\langle (G^{-1})_{00}\rangle$ on lifetime cancels out, leaving only an implicit dependence through the quantum efficiency term in R_0. Our analysis above indicates that $\tau^{-1}\langle (G^{-1})_{00}\rangle$ is minimally affected by the filament length. The other fluorophore parameters are constants for a given fluorescent fusion protein whereas the other f-actin structure parameters are generally constant. Finally, keeping actin-GFP expression roughly constant during an experiment is straightforward.

If its constituent parameters are constant, then $\tau^{-1}\langle (G^{-1})_{00}\rangle$ is a constant and Eq. 14 can be rewritten as a proportionality:

$$C_p \propto \left(1 - \frac{r}{r_m}\right) C_T. \tag{15}$$

Equation 15 relates the actin polymer concentration to the anisotropy under the constraint of constant expression level.

Imaging the anisotropy-derived actin polymerization state

Steady-state anisotropy in fixed and living HEK293 cells

Cultured HEK293 cells expressing actin-GFP (Fig. 3 *A*) were imaged either alive or after fixation. The actin-GFP anisotropy shows a region-specific variation (Fig. 3 *B*). In much of the central soma, the anisotropy is ~0.41 in both live and fixed cells (Fig. 3 *D*). Actively growing peripheral regions such as lamella/lamellipodia and filopodia exhibit a significantly reduced anisotropy. In comparison, the fluorescence anisotropy in cells expressing only GFP is spatially

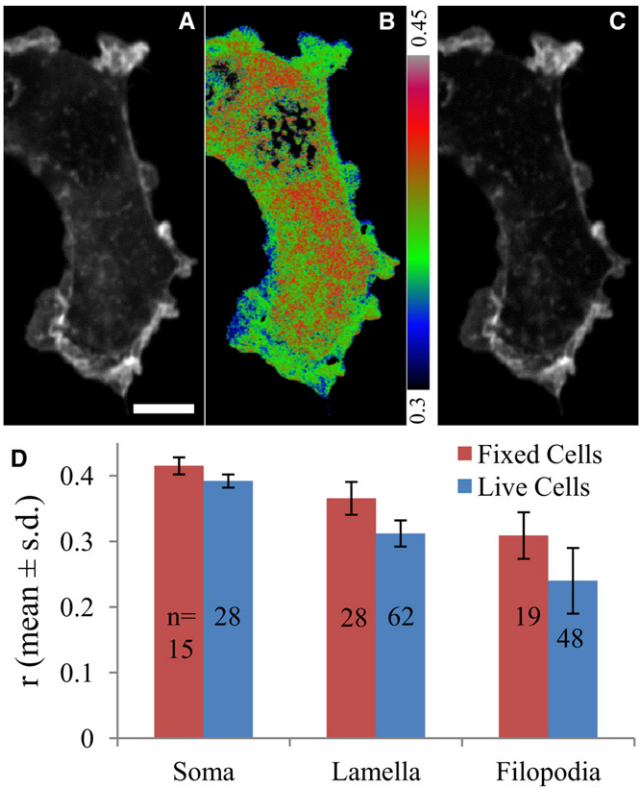

FIGURE 3 Total fluorescence intensity (*A*), anisotropy (*B*) of actin-GFP, and f-actin staining with Texas Red-X phalloidin (*C*) in a fixed HEK293 cell. (*D*) Anisotropy in both live (*red*) and fixed (*blue*) cells is spatially heterogeneous with significant decreases in regions known to be f-actin-rich. Scale bar = 10 μm.

homogenous, with an average value of 0.413 ± 0.023 (n = 23), comparable to previously published results (20).

The anisotropy of somatic actin-GFP is comparable to that of GFP alone, indicating no interaction between actin-GFPs and implying that somatic actin-GFP is monomeric. The cell periphery, on the other hand, exhibits significantly reduced anisotropy, as would be expected from actin-GFP that had incorporated into f-actin and was undergoing emFRET. The slightly lower anisotropy in the periphery of live cells compared to fixed cells is possibly due to destabilization of f-actin during fixation. These results are consistent with phalloidin stains (Fig. 3 *C*), which reveal f-actin to be low in the soma but enriched in the growing periphery.

Validation of the theoretical model in cells

Comparing the theoretical and experimental dependence of anisotropy on polymer fraction and expression level

Our theoretical model (Eq. 14) predicts a relationship between actin-GFP anisotropy and polymer fraction with a proportionality term that depends on the expression level. Although the expression level can be treated as a constant for a single cell during most experiments, it will vary from cell to cell. Validating Eq. 14 therefore requires empirically checking the relationship between anisotropy and polymer fraction for a range of expression levels.

We take the actin-GFP expression level to be proportional to the mean actin-GFP fluorescence of the extranuclear soma, i.e., $F_{soma} = \alpha[actin - GFP]$, where α is a constant for a given set of imaging parameters. Combining this with Eqs. 11 and 14, we get

$$r = r_m\left(1 - m_\ell\left(\frac{C_p}{C_T}\right)\frac{\zeta F_{soma}}{\zeta F_{soma} + 1}\right), \qquad (16)$$

where $\zeta = K_{acGFP}/(\alpha[endogenous\ g\text{-}actin])$ is assumed a constant. Equation 16 is simply a restatement of our model that can be more conveniently tested in cells. We measured the anisotropy from two types of intracellular regions in fixed HEK293 cells: lamella/lamellipodia (which are typically f-actin-rich), and actin-hotspot-free regions of the soma (which are typically f-actin-poor). In selecting regions from lamellipodia, care was taken to avoid filopodia and microspikes, as these structures contain compact bundles of f-actin that may exhibit interfilament FRET (see Discussion). For each region of interest, lamellipodium or soma, we recorded the anisotropy, r, and the mean fluorescence from the extranuclear soma of the parent cell as the corresponding measure of expression level F_{soma}. These measurements were made in a large number of cells (Lamellipodia: 138 regions of interest (ROIs) from 75 cells; Somas: 103 ROIs from 103 cells) spanning two orders of magnitude in expression level. The resulting plot of anisotropy versus expression level is shown in Fig. 4 *A* (*data points*). Each data point represents a binning (mean ± SD) of five ROIs of comparable F_{soma} values. We fit this cellular data with Eq. 16 (Fig. 4 *A*, *dashed lines*) using r_m, C_p/C_T, and ζ as fitting parameters and setting $m_\ell = 0.251$, as discussed above.

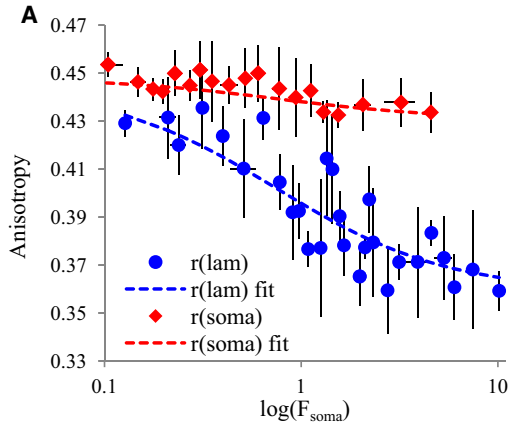

B	C_p/C_T	r_m	ζ	χ_r^2
Lam	0.77 ±0.07	0.445 ±0.010	1.3 ±0.2	1.22
Soma	0.15 ±0.04	0.448 ±0.002	1.3 fixed	0.52

FIGURE 4 Validation of the theoretical model (part 1). (*A*) The dependence of anisotropy on expression level is well fit (*dashed lines*) by our theoretical model in both f-actin-rich lamellipodia (*lam*) and f-actin poor somas (*soma*). Each data point represents a binning (mean ± SD) of 5 ROIs of comparable F_{soma} values. The best-fit values for the fit parameters are summarized in panel *B*.

The model fits the experimental data well over a large range of expression levels. Furthermore, the fit yields a polymer fraction (C_p/C_T) of 0.77 in lamellipodia and 0.15 in somas (Fig. 4 *B*), consistent with the fact that they are f-actin-rich and -poor, respectively. Our value for the polymer fraction in HEK cell lamellipodia is remarkably close to that obtained by Koestler et al. (21) ($C_p/C_T = 0.76$) in the lamellipodia of mouse melanoma cells using a very different experimental approach. Because the soma is very low in polymeric actin, there are few polymers for actin-GFP to incorporate into and hence expression level has little effect on anisotropy (Fig. 4 *A*, *red diamonds*). Conversely, lamellipodia are rich in polymeric actin that incorporates actin-GFPs and hence increasing the expression level can significantly affect the incorporation probability, energy migration, and therefore anisotropy (Fig. 4 *B*, *blue circles*). At low expression levels, actin-GFPs are unlikely to interact even if incorporated into a polymer, and hence the anisotropies from lamellipodia and somas should converge to the same value at zero expression—the anisotropy of the actin-GFP monomer. The estimates of the monomer anisotropy (Fig. 4 *B*) from lamellipodia and soma curves, 0.445 and 0.448, are indeed very close. We take the average value

from these two fits to be the actin-GFP monomer anisotropy r_m: 0.447.

The anisotropy-derived polymer concentration reproduces the phalloidin staining pattern and drug response

Having measured the actin-GFP monomer anisotropy (r_m), we can now use Eq. 15 to calculate, pixel-by-pixel, an image that is proportional to the actin polymer concentration. Furthermore, because the total actin-GFP concentration C_T is proportional to the total fluorescence intensity (F_T), we can rewrite Eq. 15 as

$$C_p(x,y,z) \propto \left(1 - \frac{r(x,y,z)}{r_m}\right) F_T(x,y,z). \qquad (17)$$

As an independent measure of the f-actin distribution, actin-GFP-expressing HEK293 cells were fixed and stained with Texas Red-X phalloidin. The anisotropy-derived actin polymer distribution could then be directly compared to the phalloidin distribution. Fig. 5 shows the calculated total fluorescence intensity, anisotropy-derived actin polymer distribution, and phalloidin stain. The anisotropy-derived polymer distribution and the phalloidin signal (Fig. 5, *B* and *C*) are highly similar, yielding very high correlation (0.89 ± 0.03, $n = 16$) and overlap coefficients (0.92 ± 0.03, $n = 16$). The anisotropy-derived polymer concentration is therefore a good indicator of the f-actin distribution. Furthermore, the near unity of its linear correlation coefficient with the phalloidin stain further validates the use of Eq. 15 and our treatment of $\tau^{-1}\langle(G^{-1})_{00}\rangle$ as a constant for a given expression level.

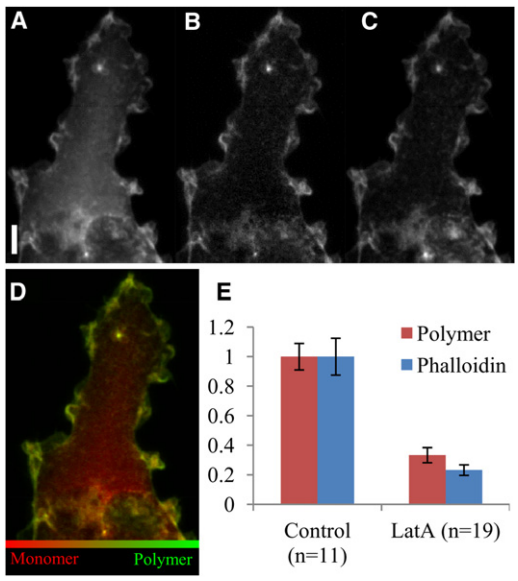

FIGURE 5 Validation of the theoretical model (part 2). Total fluorescence intensity (*A*) and the anisotropy-derived polymer concentration (*B*) of actin-GFP. Scale bar = 10 μm. The derived polymer concentration (*B*) shows a high similarity to the Texas Red-X phalloidin stain (*C*). Panels *A* and *B* can be combined in a red-green image (*D*) to visualize the monomer-polymer continuum. (*E*) Latrunculin A induces a comparable decrease in both the anisotropy-derived polymer concentration and the phalloidin signal (mean $\pm$ SD).

To facilitate visualization, we display the anisotropy-derived polymer concentration in green and the total fluorescence intensity in red (Fig. 5 *D*). It follows that a purely red pixel contains only g-actin. Pixels that are increasingly green have proportionally higher concentrations of f-actin.

To ensure that the anisotropy-derived polymer concentration responds correctly to drug-induced perturbations of the f-actin level, actin-GFP-expressing HEK293 cells were treated with the actin-destabilizing drug Latrunculin A (15 min, 1 μM) and then fixed and stained with Texas Red-X phalloidin. The anisotropy-derived polymer fraction and the phalloidin signal were then measured in single z planes near the base of the cell and found to be comparably lower in treated cells (Fig. 5 *E*) compared to control cells. Hence, the anisotropy-derived polymer concentration indicates changes in f-actin that are similar to those calculated from the gold-standard phalloidin stain.

Live imaging of the actin-polymerization state

Because our method is based on two-photon excitation, it can readily be extended to living cells and tissue. We demonstrate here imaging of the anisotropy-derived actin polymerization state in live cell cultures, acute hippocampal slices from mouse, and intact *Drosophila* larvae. To the best of our knowledge, these are the first direct images of the actin polymerization state acquired in acute hippocampal slices and in live animals. We utilize the red-green monomer-polymer display described above.

Cultured cells

In live HEK293 cells (Fig. 6 and Movie S1 in the Supporting Material), as in fixed cells, the soma appears mostly red, indicating monomeric g-actin. Lamellipodia and filopodia (Fig. 6, *B* and *C*) have higher green intensities, indicating larger polymeric f-actin concentrations. In lamellipodia, the actin polymerization state depends on whether the lamellipodium is extending or retracting—as defined by the position of the leading edge with respect to a fixed point near the base (Fig. 6 *D*, *green line*). During extension, the polymer fraction and the total actin concentration (C_T) remain roughly constant (Fig. 6 *D*) throughout the lamellipodium, with a somewhat higher polymer fraction near the leading edge. During this phase, it is common to see filopodia or microspikes that develop into filopodia (Fig. 6 *B*, *blue arrows*). During retraction, the leading edge exhibits a decrease in the polymer fraction (Fig. 6 *D*, *blue line*) but an apparent increase in the total actin concentration (Fig. 6 *D*, *red line*).

The drop in the polymer fraction at the leading edge during retraction indicates an expected destabilization of the actin cytoskeleton. In contrast, the accompanying

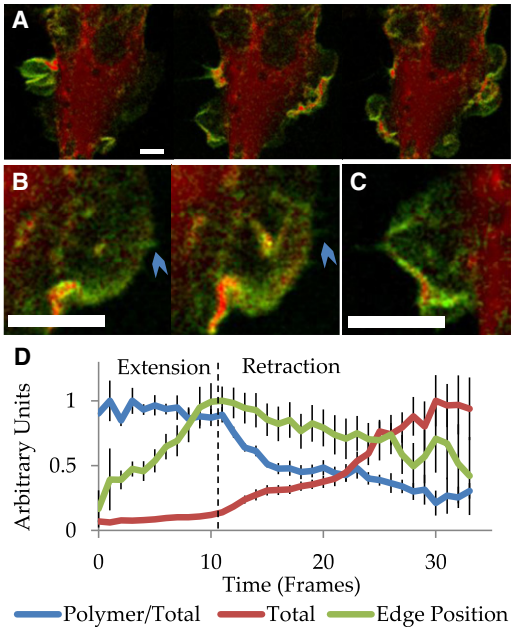

FIGURE 6 Imaging the actin polymerization state in live cells (*A*; select frames from Movie S1 in the Supporting Material). Scale bar = 10 μm. Saturated pixels (bright red) could not be used to calculate a polymer concentration and hence, have an associated green value of zero. Actin dynamics in live lamellipodia (*B* and *C*) show a high f-actin concentration near the leading edge. Actin microspikes (*B*, *blue arrow*) can be seen that develop into filopodia. The polymer fraction near the lamellar leading edge (*D*, *blue line*) is constant during extension (left of *dashed line*) but declines during retraction. The leading-edge total actin concentration (*D*, *red line*) undergoes an apparent increase during retraction. The extension and retraction phases are defined by the position of the leading edge (*D*, *green line*) with respect to a fixed point near the base.

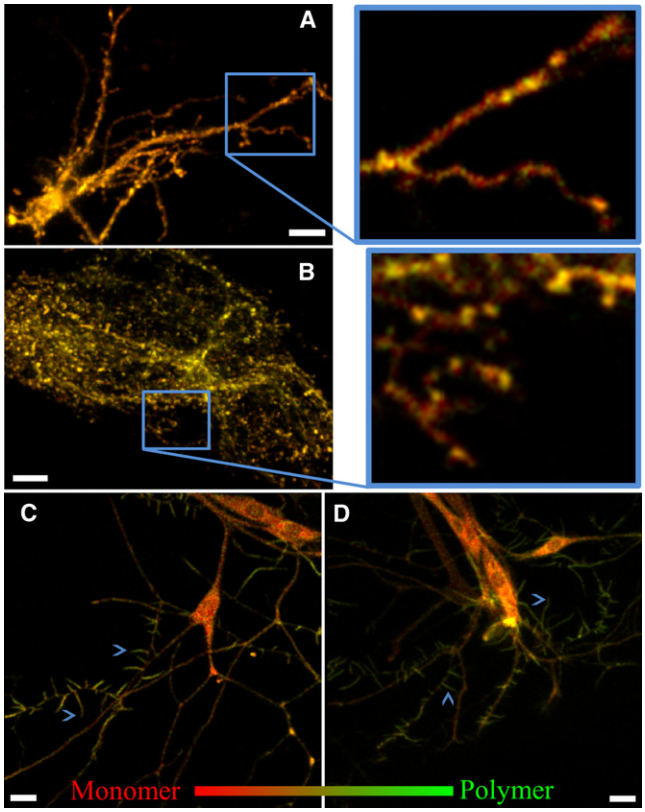

FIGURE 7 Imaging the anisotropy-derived actin polymerization state in vivo. (*A* and *B*) Live acute hippocampal slices expressing virally transduced actin-GFP. Maximal *z* projections of a granule neuron (*A*) in the dentate gyrus, and interneuron (*B*) in the stratum oriens of the CA1 layer. (*Blue highlighted boxes*) Single *z* planes. (*C* and *D*) Peripheral sensory neurons in live, intact, unanesthetized *Drosophila* larvae expressing actin-GFP selectively in peripheral sensory neurons. (*Blue arrows*) Examples of dendritic filopodia. Images are average *z* projections. Scale bars = 10 μm.

increase in the total actin signal is surprising and could be a volumetric effect due to thickening of the lamellipodium edge as it peels back from the substrate. Corrections for volume changes are often necessary in fluorescence microscopy and are typically implemented by normalizing intensity changes to those of a whole cell marker. Fluorescence anisotropy and the calculated actin polymer fraction, being inherently ratios, are immune to volumetric artifact and therefore accurately represent changes in the actin polymer fraction.

Acute hippocampal slices

We virally transduced actin-GFP in the hippocampi of adult mice and prepared acute hippocampal slices from these mice after 2–3 weeks of expression. The slices were perfused with oxygenated artificial cerebro-spinal fluid and imaged while living. We calculated images of the anisotropy-derived polymer fraction for multiple cell types (Fig. 7, *A* and *B*), including granule neurons in the dentate gyrus, and inhibitory interneurons in the CA1 layer. Both these cell types showed relatively high polymer fractions in the soma and larger neurites. Smaller, more distal neurites, however, tended to have a lower polymer fraction, punctuated by more highly polymerized compartments and terminals (Fig. 7, *A* and *B*, *blue boxes*).

Intact Drosophila larvae

We also calculated images of the anisotropy-derived polymer fraction in live, intact *Drosophila* larvae expressing actin-GFP in peripheral sensory neurons (22,23). *Drosophila* dendritic arborization sensory neurons (Fig. 7, *C* and *D*) show relatively low polymer fractions in their somas and primary dendrites. The filamentous projections from these dendrites, known as dendritic filopodia (*blue arrows*), are highly enriched in f-actin. Dendritic filopodia are believed to be the precursors of new dendrites and are common in young larvae with developing dendritic arbors (22).

In highly scattering tissue such as brain, we were practically limited to imaging at depths of $<$70 μm. Light scattering destroys fluorescence polarization and therefore reduces the dynamic range of anisotropy measurements. Because red light scatters less in tissue, we are developing

emFRET-optimized actin fusion proteins with red emissions to facilitate emFRET imaging in tissue.

DISCUSSION

Interfilament FRET in compact f-actin bundles

Actin filaments can be organized into branched networks and bundles (for review, see Revenu et al. (24)). In networks and the bundles mediated by many f-actin bundling proteins, the interfilament distance (axis-to-axis) is substantially larger than a typical Förster radius. For example, α-actinin bundles f-actin with an interfilament distance of 391 Å (25). In contrast, f-actin bundled by the smallest bundling proteins, fascin and fimbrin, has an interfilament distance as short as 120 Å (26,27). This corresponds to a ~50 Å distance of closest approach for the actin N-termini on adjacent filaments—well within FRET range. It is therefore likely that interfilament FRET in these compact bundles is comparable to, or greater than, intrafilament FRET. Fascin/fimbrin-mediated compact bundles are typically found in thin membrane protrusions such as filopodia, stereocilia, and microvilli.

Because the model presented here considers intrafilament FRET to be the sole source of depolarization, any additional depolarization due to interfilament FRET would lead to an overestimate of the true polymer concentration. This source of error is not immediately apparent in our correlations between phalloidin staining and the anisotropy-derived polymer concentration because filopodia represent a very small fraction of the total number of pixels in HEK cells. Nonetheless, an accurate calculation of the f-actin concentration in compact bundle-rich regions such as filopodia requires the development of additional theory that accounts for interfilament FRET.

The advantages of emFRET over heteroFRET

Although interactions between like proteins can be probed with either heteroFRET or emFRET, there are several advantages to using emFRET.

Incorporation probability affects the rate of energy transfer

In heteroFRET, actin-CFP and actin-YFP compete with each other for incorporation into f-actin. As a result, two potentially interacting sites can be occupied by two donors, or two acceptors, precluding FRET and reducing the ensemble average FRET rate. In emFRET, every incorporated fluorophore is both a donor and an acceptor; as a result, there are no pairs that are incapable of FRET.

The comparison becomes more realistic if we impose the constraint that the total amount of expressed actin fusion protein must be the same in both cases. Under such a constraint, a heteroFRET experiment must split the total expressed fusion protein concentration between the donor and the acceptor, effectively reducing the concentrations of both. The net effect of splitting the expressed concentration and the formation of FRET incompetent pairs is that the average FRET rate in emFRET is potentially fourfold larger than in heteroFRET (see Section S6 in the Supporting Material). As a result, emFRET can potentially generate the same rate of energy transfer as heteroFRET with fourfold less total fusion protein expression. This is of great importance given that overexpression of actin can affect cell physiology (28).

Donor/acceptor stoichiometry

Optimizing heteroFRET typically involves expressing the donor and acceptor in a specific stoichiometry. Although an obligate donor/acceptor stoichiometry is possible with specialized constructs, it generally requires optimization of transfection conditions and displays inevitable cell-to-cell variability. This is a tractable problem in cell culture but becomes increasingly difficult in tissue. In emFRET, because every GFP is both a donor and an acceptor, the stoichiometry problem is completely avoided.

Single fluorophore imaging

Using two fluorophores requires corrections for nonselective excitation and emission bleedthrough between the two detection channels (29). Anisotropy imaging utilizes only one fluorophore and hence avoids these problems altogether. Imaging with high numerical aperture objectives does cause polarization mixing; however, the correction for this is straightforward (30,31).

Indirect probes of actin polymerization state

EmFRET carries the limitations common to overexpressing any actin fusion protein. Overexpression can alter cellular actin dynamics, while the presence of a GFP tag can affect native interactions (32). As an alternative to direct probes, a number of live cell indirect probes have been developed (33–36) based on the fluorescent labeling of f-actin binding proteins and short peptides. Although these techniques are promising and increasingly used, they all involve utilizing probes that compete with endogenous f-actin binding proteins, making them sensitive to the f-actin protein binding state. Their dynamics must therefore be interpreted with some care, as their limitations remain to be fully understood (37). Furthermore, as with imaging the actin-GFP total intensity, the unbound pool of probe represents a background signal that limits the dynamic range of f-actin detection. It would be an intriguing possibility to extend anisotropy imaging to probes like Lifeact-GFP in cells and even live transgenic animals (34) to enhance their ability to detect f-actin.

CONCLUSION

The actin polymerization state has drawn intense study for its role in a diverse set of important cellular processes

ranging from cell division and migration to learning and memory. But the lack of a simple, in vivo method for directly imaging the actin polymerization state has been limiting. For example, in the brain, although the actin polymerization state undoubtedly plays a key role in learning (long-term potentiation), there are indications that both polymerization and depolymerization are necessary for long-term potentiation (5,38,39). Do these opposing polymerization dynamics arise from differing experimental conditions such as the system used (intact brain versus cultured neurons) or compartments studied (dendritic spine versus dendritic field)? Or, alternatively, does actin polymerization during synaptic plasticity have genuinely complex spatiotemporal dynamics? We seek to explore these questions by developing a simple, direct, in vivo probe of the actin polymerization state.

Finally, we note that although our method has been developed for quantitatively imaging the polymerization state of actin, it could potentially be readily extended to any polymer (microtubules, intermediate filaments, amyloids, etc.).

SUPPORTING MATERIAL

Supporting sections, two tables, five figures, one movie, and references (40–42) are available at http://www.biophysj.org/biophysj/supplemental/S0006-3495(12)00113-0.

The authors thank Mark Sonders and Jonathan Javitch (Columbia University) for the use of their multiphoton microscope. Actin-GFP adenovirus and Tet-Off virus were provided by Scott Soderling (Duke University). *Drosophila* larvae expressing actin-GFP in sensory neurons were provided by Jay Brenman (University of North Carolina, Chapel Hill) and housed and maintained by Brian McCabe and Ben Jiwon Choi (Columbia University). The polarizing beam splitter was adapted to the Prairie Ultima using a custom design by John Rafter at Prairie Technologies.

This research was supported by the Howard Hughes Medical Institute.

REFERENCES

1. Waterman-Storer, C. M., A. Desai, …, E. D. Salmon. 1998. Fluorescent speckle microscopy, a method to visualize the dynamics of protein assemblies in living cells. *Curr. Biol.* 8:1227–1230.
2. Tatavarty, V., E. J. Kim, …, J. Yu. 2009. Investigating sub-spine actin dynamics in rat hippocampal neurons with super-resolution optical imaging. *PLoS ONE.* 4:e7724.
3. Taylor, D. L., J. Reidler, …, L. Stryer. 1981. Detection of actin assembly by fluorescence energy transfer. *J. Cell Biol.* 89:362–367.
4. Marushchak, D., S. Grenklo, …, L. B. Johansson. 2007. Fluorescence depolarization studies of filamentous actin analyzed with a genetic algorithm. *Biophys. J.* 93:3291–3299.
5. Okamoto, K. I., T. Nagai, …, Y. Hayashi. 2004. Rapid and persistent modulation of actin dynamics regulates postsynaptic reorganization underlying bidirectional plasticity. *Nat. Neurosci.* 7:1104–1112.
6. Clayton, A. H. A., Q. S. Hanley, …, T. M. Jovin. 2002. Dynamic fluorescence anisotropy imaging microscopy in the frequency domain (rFLIM). *Biophys. J.* 83:1631–1649.
7. Lidke, D. S., P. Nagy, …, T. M. Jovin. 2003. Imaging molecular interactions in cells by dynamic and static fluorescence anisotropy (rFLIM and emFRET). *Biochem. Soc. Trans.* 31:1020–1027.
8. Runnels, L. W., and S. F. Scarlata. 1995. Theory and application of fluorescence homotransfer to melittin oligomerization. *Biophys. J.* 69:1569–1583.
9. Gautier, I., M. Tramier, …, M. Coppey-Moisan. 2001. Homo-FRET microscopy in living cells to measure monomer-dimer transition of GFP-tagged proteins. *Biophys. J.* 80:3000–3008.
10. Blackman, S. M., D. W. Piston, and A. H. Beth. 1998. Oligomeric state of human erythrocyte band 3 measured by fluorescence resonance energy homotransfer. *Biophys. J.* 75:1117–1130.
11. Chan, F. T. S., C. F. Kaminski, and G. S. Kaminski Schierle. 2011. HomoFRET fluorescence anisotropy imaging as a tool to study molecular self-assembly in live cells. *ChemPhysChem.* 12:500–509.
12. Varma, R., and S. Mayor. 1998. GPI-anchored proteins are organized in submicron domains at the cell surface. *Nature.* 394:798–801.
13. Blackman, S. M., C. E. Cobb, …, D. W. Piston. 1996. The orientation of eosin-5-maleimide on human erythrocyte band 3 measured by fluorescence polarization microscopy. *Biophys. J.* 71:194–208.
14. Patterson, G. H., D. W. Piston, and B. G. Barisas. 2000. Förster distances between green fluorescent protein pairs. *Anal. Biochem.* 284:438–440.
15. Miki, M., S. I. O'Donoghue, and C. G. Dos Remedios. 1992. Structure of actin observed by fluorescence resonance energy transfer spectroscopy. *J. Muscle Res. Cell Motil.* 13:132–145.
16. Zhou, H. X. 2001. Loops in proteins can be modeled as worm-like chains. *J. Phys. Chem. B.* 105:6763–6766.
17. Craver, F. W., and R. S. Knox. 1971. Theory of polarization quenching by excitation transfer. 2. Anisotropy and second-neighbor considerations. *Mol. Phys.* 22:385–402.
18. Small, J. V., M. Herzog, and K. Anderson. 1995. Actin filament organization in the fish keratocyte lamellipodium. *J. Cell Biol.* 129:1275–1286.
19. Lewis, A. K., and P. C. Bridgman. 1992. Nerve growth cone lamellipodia contain two populations of actin filaments that differ in organization and polarity. *J. Cell Biol.* 119:1219–1243.
20. Tramier, M., and M. Coppey-Moisan. 2008. Fluorescence anisotropy imaging microscopy for homo-FRET in living cells. *In* Fluorescent Proteins, 2nd Ed. Kluwer Academic, New York. 395–414.
21. Koestler, S. A., K. Rottner, …, J. V. Small. 2009. F- and G-actin concentrations in lamellipodia of moving cells. *PLoS ONE.* 4:e4810.
22. Medina, P. M. B., L. L. Swick, …, J. E. Brenman. 2006. A novel forward genetic screen for identifying mutations affecting larval neuronal dendrite development in *Drosophila melanogaster. Genetics.* 172:2325–2335.
23. Andersen, R., Y. M. Li, …, J. E. Brenman. 2005. Calcium/calmodulin-dependent protein kinase II alters structural plasticity and cytoskeletal dynamics in *Drosophila*. *J. Neurosci.* 25:8878–8888.
24. Revenu, C., R. Athman, …, D. Louvard. 2004. The co-workers of actin filaments: from cell structures to signals. *Nat. Rev. Mol. Cell Biol.* 5:635–646.
25. Taylor, K. A., D. W. Taylor, and F. Schachat. 2000. Isoforms of α-actinin from cardiac, smooth, and skeletal muscle form polar arrays of actin filaments. *J. Cell Biol.* 149:635–646.
26. Volkmann, N., D. DeRosier, …, D. Hanein. 2001. An atomic model of actin filaments cross-linked by fimbrin and its implications for bundle assembly and function. *J. Cell Biol.* 153:947–956.
27. Sedeh, R. S., A. A. Fedorov, …, M. Bathe. 2010. Structure, evolutionary conservation, and conformational dynamics of *Homo sapiens* fascin-1, an F-actin crosslinking protein. *J. Mol. Biol.* 400:589–604.
28. Peckham, M., G. Miller, …, G. A. Dunn. 2001. Specific changes to the mechanism of cell locomotion induced by overexpression of β-actin. *J. Cell Sci.* 114:1367–1377.
29. Okamoto, K.-I., and Y. Hayashi. 2006. Visualization of F-actin and G-actin equilibrium using fluorescence resonance energy transfer (FRET) in cultured cells and neurons in slices. *Nat. Protoc.* 1:911–919.

30. Axelrod, D. 1979. Carbocyanine dye orientation in red cell membrane studied by microscopic fluorescence polarization. *Biophys. J.* 26: 557–573.

31. Axelrod, D. 1989. Fluorescence polarization microscopy. *Methods Cell Biol.* 30:333–352.

32. Wu, J.-Q., and T. D. Pollard. 2005. Counting cytokinesis proteins globally and locally in fission yeast. *Science.* 310:310–314.

33. Riedl, J., A. H. Crevenna, …, R. Wedlich-Soldner. 2008. Lifeact: a versatile marker to visualize F-actin. *Nat. Methods.* 5:605–607.

34. Riedl, J., K. C. Flynn, …, R. Wedlich-Söldner. 2010. Lifeact mice for studying F-actin dynamics. *Nat. Methods.* 7:168–169.

35. Burkel, B. M., G. von Dassow, and W. M. Bement. 2007. Versatile fluorescent probes for actin filaments based on the actin-binding domain of utrophin. *Cell Motil. Cytoskeleton.* 64:822–832.

36. Dutta, D., J. W. Bloor, …, D. P. Kiehart. 2002. Real-time imaging of morphogenetic movements in *Drosophila* using Gal4-UAS-driven expression of GFP fused to the actin-binding domain of moesin. *Genesis.* 34:146–151.

37. Munsie, L. N., N. Caron, …, R. Truant. 2009. Lifeact cannot visualize some forms of stress-induced twisted F-actin. *Nat. Methods.* 7:605–607.

38. Ouyang, Y., M. Wong, …, D. W. Choi. 2005. Transient decrease in F-actin may be necessary for translocation of proteins into dendritic spines. *Eur. J. Neurosci.* 22:2995–3005.

39. Kim, C. H., and J. E. Lisman. 1999. A role of actin filament in synaptic transmission and long-term potentiation. *J. Neurosci.* 19:4314–4324.

40. Evers, T. H., E. M. W. M. van Dongen, …, M. Merkx. 2006. Quantitative understanding of the energy transfer between fluorescent proteins connected via flexible peptide linkers. *Biochemistry.* 45:13183–13192.

41. Lepine, Y., and A. Caille. 1978. Configuration of a polymer-chain interacting with a plane interface. *Can. J. Phys.* 56:403–408.

42. Lakowicz, J. R. 1999. Principles of Fluorescence Spectroscopy. Springer, New York.